Structural Characterization of Aromatic−Aromatic Complexes by Rotational Coherence Spectroscopy

Paul W. Joireman,[†] Shane M. Ohline,[‡] and Peter M. Felker*

Department of Chemistry and Biochemistry, University of California, Los Angeles, California 90095-1569

Received: January 23, 1998

Rotational coherence spectroscopy (RCS) has been applied in structural studies of (a) aromatic−aromatic van der Waals complexes of the form M−X, where M = perylene or fluorene and X = benzene or toluene, and (b) aromatic−aliphatic hydrocarbon dimers of the form M−Y, where M is as above and Y = cyclohexane or methylcyclohexane. For all of the perylene complexes the experimentally determined rotational constants are found to be consistent with centrally bound, parallel-stacked structures in which the monomer planes are separated by a distance of 3.5−4.3 A. Analogous geometries also characterize the fluorene−aliphatic species. However, the two fluorene−aromatic complexes have structures that depart from the parallel-stacked form. Both species have slipped geometries in which the monomer planes are not directly over one another. And, in the case of fluorene−benzene, the two aromatic planes are tilted with respect to one another. These differences are attributed to the significant contribution of electrostatic forces in determining the fluorene−aromatic geometries.

I. Introduction

Interactions between aromatic moieties are important in many chemical systems and processes. These include, in principle, any condensed-phase system in which aromatic species are present. More specific examples include photosynthesis,[1] porphyrin aggregation,[2] molecular recognition,[3] drug intercalation into DNA,[4] stabilization of the DNA double helix,[5] protein structure and function,[6] and electron- and energy-transfer processes.[7] The prevalence of aromatic−aromatic interactions provides a strong impetus to understand their details by studying the properties of aromatic−aromatic dimers in the gas phase. A large body of such work has indeed been reported. However, experimental information pertaining to a central property of these dimers, their geometries, has been somewhat scarce. The problem is that the species of interest tend to be too large to study by most methods of rotational spectroscopy. This has limited rotationally resolved studies to dimers of single-ring aromatics, such as (*s*-tetrazine)$_2$,[8a,b] *s*-tetrazine−benzene,[8a] (dimethyl-*s*-tetrazine)$_2$,[8a,c] and benzene dimer.[9] While these studies are certainly important to the characterization of aromatic−aromatic interactions, it is clear that a complete picture requires the study of larger species.

Rotational coherence spectroscopy (RCS)[10] has been shown to be a powerful means by which to obtain rotational constants and structural information on large, gas-phase species, including aromatic−aromatic dimers. For example, preliminary RCS results from this laboratory on the fluorene−benzene[11] and perylene−benzene[12] species have previously been reported. In addition, RCS studies of complexes of perylene with naphthalene, benzene, and substituted benzenes have been reported by Topp et al.[13] In this paper we expand upon our previous RCS studies of aromatic−aromatic dimers and present a full account of work on perylene−benzene, perylene−toluene, fluorene−benzene, and fluorene−toluene. We also report RCS results on the four aromatic−saturated-hydrocarbon dimers perylene−cyclohexane and −methylcyclohexane, and fluorene−cyclohexane and −methylcyclohexane. The structural results on these latter species provide an important point of reference from which the aromatic−aromatic structures can be considered.

The main issue that we try to address with the experimental results presented herein involves the types of forces that play a role in interaromatic interactions and the situations under which one type dominates over the others. Work by others (for example, see refs 14−18) has indicated that three kinds of forces are most important in deciding the minimum-energy geometry of an aromatic−aromatic dimer composed of nonpolar moieties. Exchange-repulsion forces determine the closest nonbonded atom−atom contacts that can occur. Attractive dispersion forces favor geometries that maximize the number of atom−atom contacts, that is, parallel-stacked ("sandwich") structures. Finally, electrostatic forces tend to favor T-shaped geometries, in which the positive charge in the plane of one moiety interacts with the negative π-electron cloud of the other moiety. They disfavor parallel-stacked geometries because of Coulomb repulsion between π clouds. Evidently, the dispersion and electrostatic forces give rise to competing demands in regard to the geometry that an aromatic−aromatic dimer adopts. The balance between these demands may be expected to change as the characteristics of the aromatics change.

Previous structural results on fluorene−benzene and perylene−benzene[12] have been interpreted as representing two different cases in regard to the interplay between dispersion and electrostatic forces in determining aromatic−aromatic geometries. Perylene−benzene has a structure quite close to parallel-stacked, in spite of the fact that calculations[16] have predicted such a geometry to be disfavored by electrostatic contributions to the intermolecular potential energy. In this complex, therefore, dispersion forces apparently dominate over electrostatic ones.[15] In contrast, the fluorene−benzene geometry—an approximate parallel-displaced one in which the planes of the

[†] Present address: Department of Chemistry, Hamilton College, 198 College Hill Rd., Clinton, NY 13323.

[‡] Department of Chemistry, Wellesley College, Wellesley, MA 02181.

S1089-5639(98)00867-6 CCC: $15.00
Published on Web 05/21/1998

aromatic moieties are at a small but significant angle to one another—indicates that neither electrostatic nor dispersion forces are dominant in determining the structure.

The results reported in the present paper provide further evidence for these interpretations. The perylene− and fluorene−toluene results show that these species have geometries similar to their benzene counterparts. Thus, they suggest a prevalence for the parallel-stacked and parallel-displaced structural types in perylene−aromatic and fluorene−aromatic complexes, respectively. The results on the aromatic−cyclohexane and aromatic−methylcyclohexane complexes are also informative. The motivation for studying these complexes stems from the fact that the cyclohexanes have sizes similar to benzene and toluene and thus should have similar dispersion interactions with perylene and fluorene. However, they also have no π electrons, so that electrostatic repulsion between π-electron clouds can play no role in determining the geometries of complexes involving them. A comparison of the geometries of the benzene and toluene complexes with those of the cyclohexane and methylcyclohexane complexes therefore sheds light on the importance of electrostatic forces in determining the geometries of the aromatic−aromatic species. Our results confirm that these forces do play a significant role in fluorene−benzene and −toluene and much less of a role in the corresponding perylene complexes.

The organization of the paper is as follows. Section II is an experimental section in which the implementation of RCS and the pertinent data analysis are explained. Section III presents the experimental results for all of the complexes studied. Section IV pertains to a consideration of the geometries that are consistent with the RCS data. Finally, section V is a discussion of what the structural results imply about the intermolecular forces that bind the species.

II. Experimental Section

A. Fluorescence Excitation Spectroscopy. The $S_1 \leftrightarrow S_0$ vibronic spectroscopy of several of the species of interest herein has not previously been reported. Thus, we measured the fluorescence excitation spectra for these complexes. The laser apparatus used to obtain these spectra consisted of an injection-seeded Q-switched Nd:YAG laser, the frequency-doubled output of which pumped a scanning dye laser. The output of the dye laser was directed through an autotracking frequency-doubling crystal. The ultraviolet output was attenuated and directed into the same molecular-beam chamber as used for the RCS experiments. The molecular-beam expansion conditions and the fluorescence detection procedures for the fluorescence excitation experiments were identical to those used in the RCS studies- of the complexes (as described below). A fluorescence excitation spectrum was measured by detecting total fluorescence as a function of the wavelength of the dye laser. Spectral resolution was about 0.5 cm^{-1}.

B. Rotational Coherence Spectroscopy. RCS experiments were performed by using the technique of time-resolved fluorescence depletion (TRFD).[19] Since the apparatus has been described in detail elsewhere,[20] only a brief description is given here. The frequency-doubled output of a Q-switched mode-locked Nd:YAG laser was used to synchronously pump a cavity-dumped dye laser (1 kHz repetition rate). The dye-laser output was then used in one of the following ways. In experiments on perylene complexes it was combined collinearly with the fundamental of the Nd:YAG laser and directed through a β-barium borate (BBO) crystal to create excitation pulses by sum-frequency generation. In experiments involving fluorene complexes it was frequency-doubled directly by the BBO crystal. In both cases the BBO output was sent through a Michelson interferometer to obtain pump and variably delayed probe pulses of approximately equal intensity. The pump and probe pulse trains, polarized parallel to one another, were recombined at the output of the interferometer and were gently focused into the supersonic molecular-beam sample a few millimeters downstream from the expansion orifice of the molecular beam.

The continuous free jet was formed as follows. Helium at 130−150 psig passed over a room-temperature sample of benzene, toluene, cyclohexane, or methylcyclohexane and was then combined through a needle valve with the main carrier gas flow (helium at 70−90 psig). The resulting gas mixture passed over a heated sample of perylene (200 °C) or fluorene (110 °C) contained in a Pyrex tube. This mixture expanded through a $\sim$50 μm diameter orifice into a vacuum chamber maintained at $\sim 10^{-4}$ Torr. The resulting seeded, supersonic expansion was the sample in all of the experiments reported here.

Spectrally integrated laser-induced fluorescence was collected by an elliptical mirror arrangements and detected by a photomultiplier tube. The output of the photomultiplier was temporally integrated and averaged by a boxcar integrator. The boxcar output was recorded by a computer as a function of pump−probe delay to yield a TRFD trace. A typical completed scan corresponds to the average of 10 or more individual traces, each of which was obtained by averaging 300 laser shots at each delay position.

RCS traces for 36 distinct species were measured, corresponding to various deuterated isotopomers of the eight different complexes. We shall denote these different isotopomers by using the labeling convention $h(d)_n-h(d)_m$, where n and m designate the number of protons (deuterons) on the two monomers composing the complex. (For example, the $h_{10}-d_6$ isotopomer of fluorene−benzene is the one composed of perprotonated fluorene and perdeuterated benzene.) Whenever d_3 is used in such a way, it is meant to denote toluene with its methyl group fully deuterated. Perylene and fluorene (both from Sigma) and benzene, toluene, cyclohexane, and methylcyclohexane (all from Aldrich) were used without further purification. The deuterated derivatives of these molecules were obtained from Cambridge Isotope Laboratories.

All RCS traces were obtained by tuning the picosecond laser to the perylene− or fluorene−localized $S_1 \leftrightarrow S_0$ 0_0^0 band of the pertinent complex. The frequencies for most of these transitions were taken from the literature.[15,22,23] Those that were unavailable were obtained by measuring fluorescence excitation spectra. RCS-TRFD traces were analyzed by first removing the baseline that enters into them. Rotational constants were then extracted from the traces in the following way. First, RCS transients present in the data were assigned. Preliminary values for various rotational constants were determined from the positions of these transients. The traces were then fit to theory[24] by using a nonlinear least-squares method[25] in which the values of the rotational constants served as fitting parameters. In these fits the temperature (5 K), the temporal response function of the system ($\Delta t \sim 32$ ps fwhm Gaussian), and the transition dipole direction were held fixed. The best-fit rotational constants obtained in this way are the ones that we report below.

In RCS-TRFD experiments both ground- and excited-state rotational coherences are probed.[24] In situations where the diflferences between the rotational constants in the two states

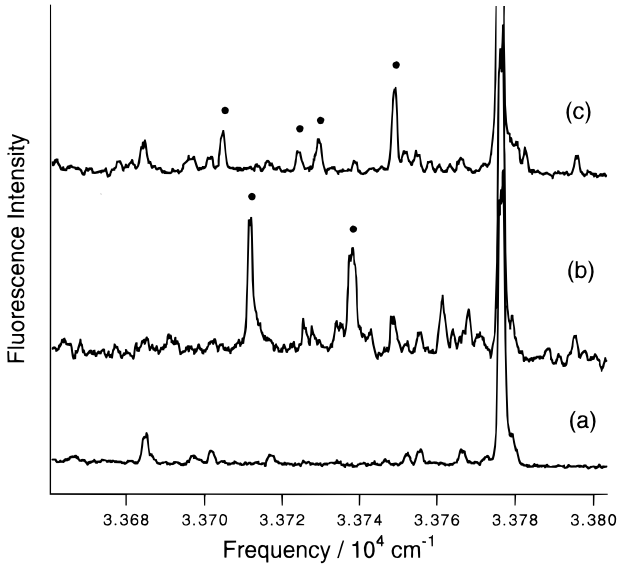

Figure 1. Fluorescence excitation spectra of expansions of (a) fluorene, (b) fluorene and cyclohexane, and (c) fluorene and methylcyclohexane, each seeded in helium. The bands labeled with dots in (b) and (c) are cyclohexane- or methylcyclohexane-dependent bands, respectively.

are small enough that transients due to the former coherences cannot be resolved from those due to the latter, one obtains the average of ground- and excited-state rotational constants from the analysis of a TRFD trace. This situation holds for all of the complexes studied herein with the exception of fluorene−benzene. In the fluorene−benzene results, coherence effects from the two states have been resolved. State-specific rotational constants are therefore quoted for the isotopomers of this species.

III. Results

A. Fluorescence Excitation Spectra. Figure 1 shows fluorescence excitation spectra corresponding to seeded expansions of (a) fluorene, (b) fluorene/cyclohexane, and (c) fluorene/methylcyclohexane. The large peak at 33 777 cm^{-1} in all of these spectra is fluorene's $S_1 \leftarrow S_0$ 0_0^0 band.[26] The features denoted with a • in Figure 1b,c are dependent upon the partial pressures of cyclohexane and methylcyclohexane, respectively. Hence, we assign these bands to the respective fluorene−X complexes. Since other spectra taken from 125 to 275 cm^{-1} to the red of the fluorene 0_0^0 reveal no additional absorption bands, we assign the red-most cyclohexane- and methylcyclohexane-dependent bands at −65 and −72 cm^{-1}, respectively, to the 0_0^0 bands of the pertinent fluorene−X one-to-one complexes. Notably, RCS traces measured for both of the cyclohexane-dependent peaks in Figure 1b were found to be identical. Similarly, RCS traces corresponding to each of the methylcyclohexane-dependent bands in Figure 1c were found to be indistinguishable from one another.

The $S_1 \leftrightarrow S_0$ 0_0^0 transition frequency of perylene−toluene was obtained from a fluorescence excitation scan of the picosecond dye laser. A toluene-dependent resonance found at 23 612 cm^{-1} was assigned to the 0_0^0 band for three reasons. First, its red shift from the bare perylene 0_0^0 band is comparable to that for perylene−benzene.[15] Second, there are no observable toluene-dependent resonances further red-shifted from this peak. Third, a toluene-dependent resonance at 353 cm^{-1} to the blue of our assigned 0_0^0 was also observed. The 353 cm^{-1} interval is known to correspond to an S_1 vibrational mode of perylene that has substantial activity in the $S_1 \leftarrow S_0$ vibronic spectrum.[15,27]

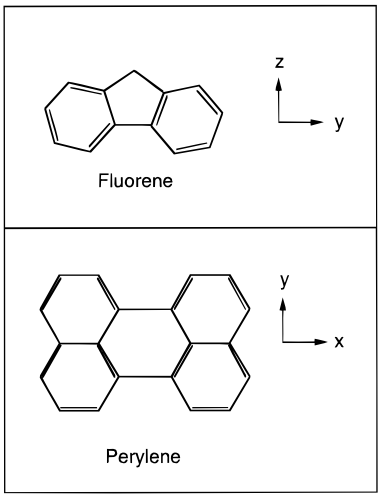

Figure 2. Structural formulas for perylene and fluorene. The right-handed axis systems used herein are also shown (origins are fixed to the molecular centers of mass).

B. RCS of Perylene Complexes. The transition dipole of the perylene $S_1 \leftarrow S_0$ 0_0^0 band lies along the long axis of the molecule, or the *x*-axis as defined in Figure 2a. The band appears at $\bar{\nu} = 24\,065$ cm^{-1} for the perprotonated species[27] and $\bar{\nu} = 24\,115$ cm^{-1} for the perdeuterated species.[28] Transition frequencies for each complex are given in the figure captions corresponding to their experimental traces. RCS results for four isotopomers of perylene−benzene have been reported previously.[12] RCS-TRFD experimental traces for selected isotopomers of perylene−X complexes where X = toluene, cyclohexane, and methylcyclohexane are shown in Figures 3−6, respectively. In all cases, the data obtained for the other isotopomers of each complex exhibit analogous features.

All perylene−X complexes exhibit two noticeable transients, in addition to that at $t = 0$, cf. Figure 1 of ref 12, and Figures 3a, 4, and 6a. These two features are equally spaced and are thus assignable to one transient type. Their alternating polarity, together with the relative magnitude of the positive- and negative-going features, clearly points to their assignment as J-type. In addition to these features, a weak transient, appearing at a slightly longer delay than the positive-polarity J-type transient, is observed for perylene−benzene (cf. Figure 2 of ref 12) and perylene−cyclohexane (cf. Figure 5). The position and magnitude of this small feature suggest that it is a C-type asymmetry transient.[30] Comparison of calculated traces with experimental ones confirms the identity of the suspected asymmetry transient as being C-type. Figure 5 shows such a comparison between experimental and calculated traces for two different isotopomers of the perylene−cyclohexane dimer. The position and appearance of the C-type transient is clearly affected by small changes in the value of $(B - C)$. This behavior allows us to extract values for $(B - C)$ from the data and estimate the uncertainty associated with such values. Although this small feature is not present in the case of perylene−toluene or perylene−methylcyclohexane, its absence is still useful. A comparison between the experimental trace and several traces calculated for fixed $(B + C)$ and variable $(B - C)$ for both perylene−toluene and perylene−methylcyclohexane is shown in Figure 3b and Figure 6b, respectively. Clearly, the C-type transient grows in with increasing asymmetry. This information can be used to place an upper bound on the value of $(B - C)$ for these complexes.

The dominant presence of J-type transients with only weak or nonexistent C-type asymmetry transients provides strong

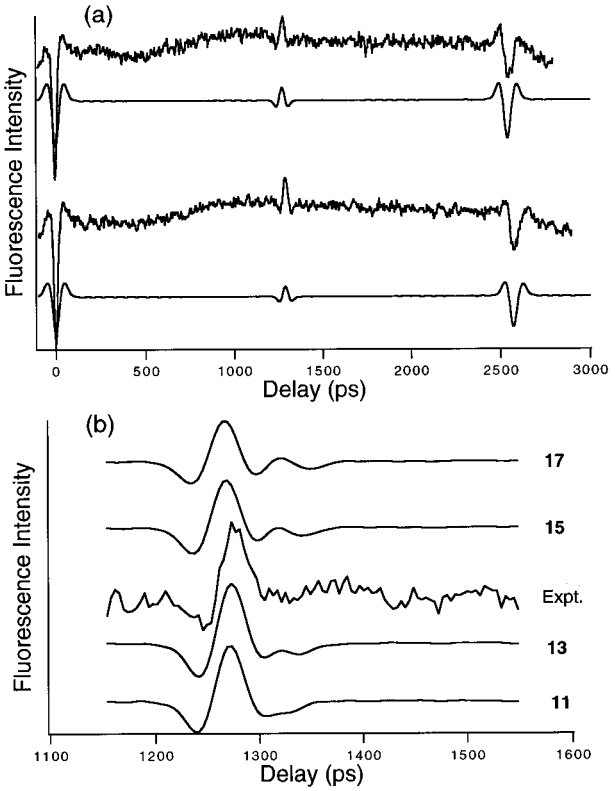

Figure 3. (a) Measured and fitted RCS-TRFD traces for the $h_{12}-h_8$ (top) and $h_{12}-d_3$ (bottom) perylene−toluene complexes. (b) Comparison of an RCS-TRFD trace (middle) measured for the $h_{12}-h_8$ isotopomer in the region of the species' first positive-polarity transient with four traces calculated by using different values of $(B - C)$, as given (in MHz). The values employed for $(B + C) = 393$ MHz and $(2A - B - C) = 158$ MHz are the same for all the calculated traces.

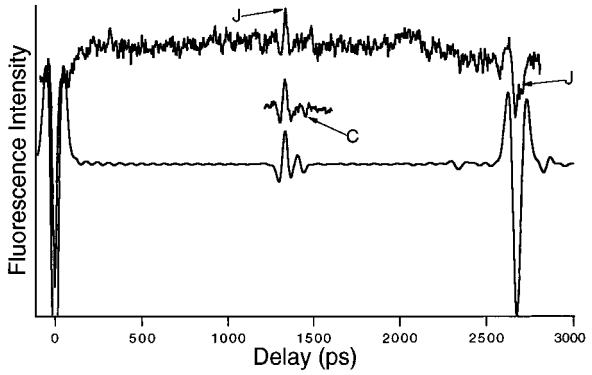

Figure 4. Top: Measured RCS-TRFD trace for the perylene−cyclohexane $h_{12}-h_{12}$ isotopomer. Middle: Higher signal-to-noise trace for the same species taken in the region of the first J-type transient, which clearly shows the presence of a C-type transient (labeled). Bottom: Trace calculated by using the rotational constant values given in the third column of Table 3 for this isotopomer, together with $(2A - B - C) = 137$ MHz.

evidence that the transition dipole is parallel-type for all perylene complexes. If the transition dipole were hybrid or perpendicular-type, hybrid transients or K-type transients,[10] respectively, would be expected. Assuming that the transition dipole is parallel-type effectively rules out any geometry that is not prolate-like with its transition moment along the *a* principal axis of the complex. Using these two pieces of information, fits were performed to the RCS data. These fits produced values of $(B + C)$ from the positions of the observed J-type transients and $(B - C)$ from the positions of the observed C-type transients. As described above, when C-type transients were not observed,

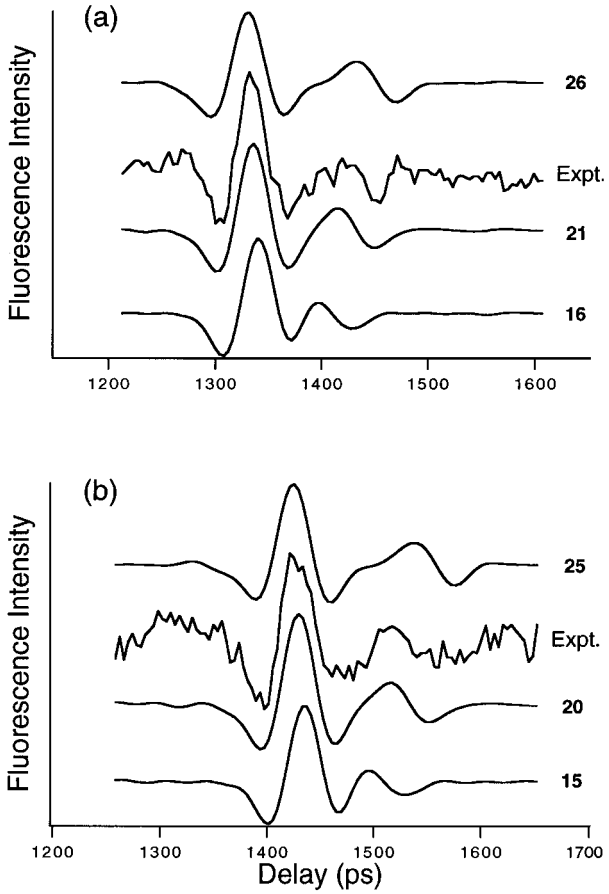

Figure 5. Experimental and calculated traces in the region of the first J-type transient for the (a) $h_{12}-h_{12}$ and (b) $d_{12}-h_{12}$ perylene−cyclohexane isotopomers. In both (a) and (b) the calculated traces are labeled by the value of $(B - C)$ (in MHz) used to calculate that trace. The other rotational constants employed for the calculations were (a) $(B + C) = 371$ MHz and $(2A - B - C) = 137$ MHz and (b) $(B + C) = 346$ MHz and $(2A - B - C) = 130$ MHz.

a comparison of calculated traces with experimental ones allowed an upper bound to be obtained for $(B - C)$. The experimentally obtained rotational constants for perylene−benzene, perylene−toluene, perylene−cyclohexane, and perylene−methylcyclohexane are reproduced in the second column of Tables 1−4, respectively.

C. RCS of Fluorene Complexes. The transition dipole of the fluorene $S_1 \leftarrow S_0$ 0_0^0 band lies along the long (y) axis of the molecule, shown in Figure 2b. The transition appears at $\bar{\nu} = 33\,777$ cm^{-1} for the perprotonated species[26] and at $\bar{\nu} = 33\,902$ cm^{-1} for the perdeuterated species.[31] Transition frequencies for each complex are given in the figure captions corresponding to their experimental traces.

1. Fluorene−Aromatic Complexes. RCS results for fluorene−benzene isotopomers are shown in Figures 7 and 8. Analgous results for fluorene−toluene isotopomers are shown in Figure 9, respectively. Results obtained for the other isotopomers of these complexes are similar to those in these figures. RCS results on fluorene−benzene have been reported previously,[11] and the transients appearing in the case of fluorene−toluene are nearly identical. The experimental traces show three different types of RCS transients: (1) a set of alternating polarity transients, (2) a set of negative polarity transients, and (3) a set of transients with dispersion line shapes. The first set of transients is assigned as J-type due to the relative magnitudes of the positive and negative polarity transients. The second set of transients is assigned as K-type

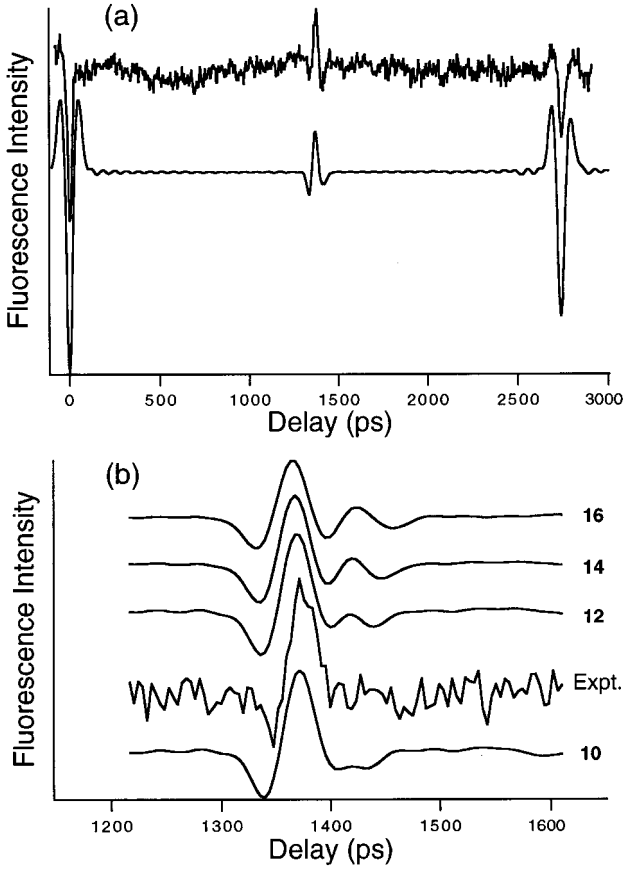

Figure 6. (a) Experimental (top) and calculated (bottom) RCS-TRFD traces for the $h_{12}-h_{14}$ isotopomer of perylene−methylcyclohexane. The $(B + C)$ and $(B - C)$ values used to generate the calculated trace are given in Table 4, third column. Further the value of $(2A - B - C)$ was taken as 106 MHz. (b) Comparison of a measured RCS trace and calculated ones in the region of the first J-type transient of the $h_{12}-h_{14}$ species. The calculated traces are labeled by the $(B - C)$ values (in MHz) used to generate them. The values of $(2A - B - C)$ and $(B + C)$ corresponding to the calculated traces are 106 and 364 MHz, respectively.

TABLE 1: Measured and Calculated Rotational Constants for Perylene−Benzene. The Estimated Uncertainties in $B + C$ and $B - C$ are ±0.75% and ±20%. The Geometry Associated with the Calculated Rotational Constants Is Shown in Figure 12

isotopomer	measured (MHz)	calculated (MHz)
$h_{12}-h_6$		
$B + C$	413	413
$B - C$	21	22
$h_{12}-d_6$		
$B + C$	404	404
$B - C$	20	20
$d_{12}-h_6$		
$B + C$	385	383
$B - C$	24	25
$d_{12}-d_6$		
$B + C$	376	376
$B - C$	24	23

due to their polarity and width,[10] and the third set is assigned as C-type asymmetry transients due to their line-shape characteristics.[30] These transient sets are labeled appropriately in Figures 7 and 9.

A new observation for fluorene−benzene is that of clear splittings in the J-type features starting with the second, negative-polarity transient at ≃2400 ps, Figure 7. This splitting is not observed in the case of fluorene−toluene. Expanded views of these split transients are shown in Figure 8 for the

TABLE 2: Measured and Calculated Rotational Constants for Perylene−Toluene. The Estimated Uncertainty in $B + C$ is ±0.75%. The Constants Given for Geometries 1 and 2 Correspond to the Structures Shown in Figure 13a,b

isotopomer	measured (MHz)	geometry 1 (MHz)	geometry 2 (MHz)
$h_{12}-h_8$			
$B + C$	392	393	393
$B - C$	<17	6	6
$h_{12}-d_3$			
$B + C$	388	388	388
$B - C$	<17	6	7
$h_{12}-d_8$			
$B + C$	381	382	382
$B - C$	<17	4	5
$d_{12}-h_8$			
$B + C$	367	365	365
$B - C$	<17	11	11
$d_{12}-d_3$			
$B + C$	362	361	361
$B - C$	<17	11	11
$d_{12}-d_8$			
$B + C$	357	356	356
$B - C$	<17	9	9

TABLE 3: Measured and Calculated Rotational Constants for Perylene−Cyclohexane. The Estimated Uncertainties in $B + C$ and $B - C$ Are ±0.75% and ±25%. The Calculated Constants Correspond to the Structure Shown in Figure 14

isotopomer	measured (MHz)	calculated (MHz)
$h_{12}-h_{12}$		
$B + C$	371	371
$B - C$	21	20
$h_{12}-d_{12}$		
$B + C$	355	355
$B - C$	20	22
$d_{12}-h_{12}$		
$B + C$	346	346
$B - C$	20	17
$d_{12}-d_{12}$		
$B + C$	333	332
$B - C$	16	18

TABLE 4: Measured and Calculated Rotational Constants for Perylene−Methylcyclohexane. The Estimated Uncertainty in $B + C$ is ±0.75%. The Geometry Associated with the Calculated Constants Is Shown in Figure 15

isotopomer	measured (MHz)	calculated (MHz)
$h_{12}-h_{14}$		
$B + C$	364	364
$B - C$	<15	9
$h_{12}-d_{14}$		
$B + C$	349	348
$B - C$	<15	13
$d_{12}-h_{14}$		
$B + C$	340	340
$B - C$	<15	4
$d_{12}-d_{14}$		
$B + C$	326	326
$B - C$	<15	7

$d_{10}-d_6$, isotopomer. Analogous splittings were observed for the other three isotopomers of fluorene−benzene studied. Two facts about these split transients are noteworthy. First, the splittings increase with increasing pump−probe delay. Second, the delay corresponding to the center of a given splitting occurs at an integer multiple of the position of the first negative J-type transient for that isotopomer. This behavior suggests either that (a) signal from two isomers of a given isotopomer are contributing to the RCS trace or (b) the ground- and excited-state values of $(B + C)$ are different enough in fluorene−benzene that the

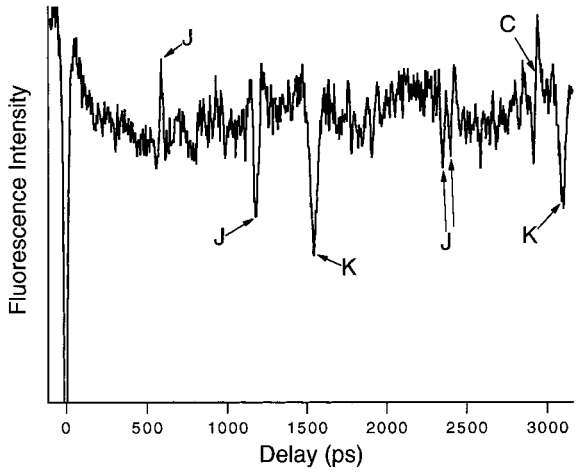

Figure 7. Measured RCS-TRFD trace for the $h_{12}-d_6$ isotopomer of fluorene−benzene. The transient types are identified in the trace by the labeling with J, K, or C.

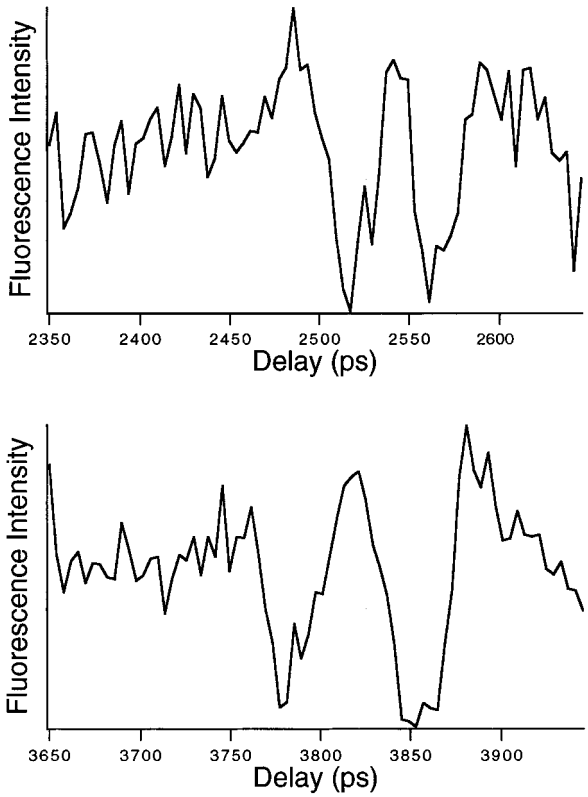

Figure 8. Measured RCS-TRFD traces for the $d_{10}-d_6$ isotopomer of fluorene−benzene in the regions of the second (top) and third (bottom) negative-polarity J-type transients.

J-type transients arising from these two states can be resolved.[24] Fluorescence excitation spectra of the isotopomers, together with the fact that the split transients have equal-intensity components, suggest that the latter possibility is actually the case. The two splitting components are therefore assigned as J-type transients for the vibrationless levels of the S_0 and S_1 states.

To obtain rotational constants for the fluorene−aromatic systems from the RCS results we assume that each complex has an oblate-like geometry, since no reasonable prolate-like structures are consistent with the RCS data. With this assumption one extracts values for $(2C - A - B)$ and $(A + B)$ and an upper bound to values of $(A - B)$ from the data. The RCS-derived rotational constants for the fluorene−benzene and fluorene−toluene isotopomers are given in Tables 5 and 6,

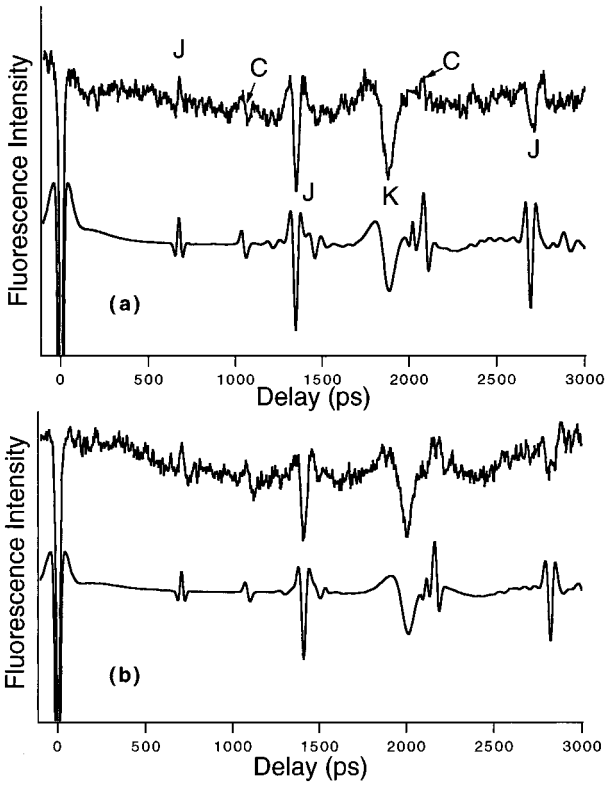

Figure 9. Experimental (top) and calculated (bottom) RCS-TRFD traces for the (a) $d_{10}-h_8$ and (b) $d_{10}-d_8$ isotopomers of fluorene−toluene. The rotational constants used for the two calculated traces are given in the third column of Table 6.

TABLE 5: Measured and Calculated Rotational Constants for the Ground- and Excited-State Geometries of Fluorene−Benzene. The Estimated Uncertainties in $(2C - A - B)$ and $(A - B)$ Are ±0.5% and ±0.4%. The Geometry Associated with the Calculated S_0 Constants Is Shown in Figure 16. That Associated with the S_1 Constants Is Described in the Text

isotopomer	measured (MHz)	calculated (MHz)
$h_{10}-h_6$		
$(2C - A - B)$	−337	−336
$(A + B)_{S_0}$	868	868
$(A - B)_{S_0}$	<30	7
$(A + B)_{S_1}$	885	884
$(A - B)_{S_1}$	<30	13
$h_{10}-d_6$		
$(2C - A - B)$	−324	−325
$(A + B)_{S_0}$	835	837
$(A - B)_{S_0}$	<30	15
$(A + B)_{S_1}$	850	852
$(A - B)_{S_1}$	<30	5
$d_{10}-h_6$		
$(2C - A - B)$	−304	−305
$(A + B)_{S_0}$	806	806
$(A - B)_{S_0}$	<30	19
$(A + B)_{S_1}$	817	820
$(A - B)_{S_1}$	<30	29
$d_{10}-d_6$		
$(2C - A - B)$	−296	−295
$(A + B)_{S_0}$	779	778
$(A - B)_{S_0}$	<30	8
$(A + B)_{S_1}$	794	792
$(A - B)_{S_1}$	<30	16

respectively. For fluorene−benzene, vibronic-state-specific values are quoted only for $(A + B)$, because resolvable splittings were only found for J-type features. The smaller $(A + B)$ values have been assigned as S_0 rotational constants. Though there is nothing in the RCS results that dictates such an assignment,

TABLE 6: Measured and Calculated Rotational Constants for the Fluorene−Toluene. The Estimated Uncertainties in ($2C - A - B$) and ($A - B$) are ±0.5%. The Geometry Associated with the Calculated Rotational Constants Is Shown in Figure 17

isotopomer	measured (MHz)	calculated (MHz)
$h_{10}-h_8$		
$(2C - A - B)$	−288	−288
$(A + B)$	794	794
$(A - B)$	<25	8
$h_{10}-d_3$		
$(2C - A - B)$	−277	−277
$(A + B)$	783	780
$(A - B)$	<25	10
$h_{10}-d_8$		
$(2C - A - B)$	−268	−268
$(A + B)$	757	757
$(A - B)$	<25	12
$d_{10}-h_8$		
$(2C - A - B)$	−267	−266
$(A + B)$	741	743
$(A - B)$	<25	10
$d_{10}-d_3$		
$(2C - A - B)$	−257	−257
$(A + B)$	730	730
$(A - B)$	<25	13
$d_{10}-d_8$		
$(2C - A - B)$	−249	−249
$(A + B)$	710	709
$(A - B)$	<25	6

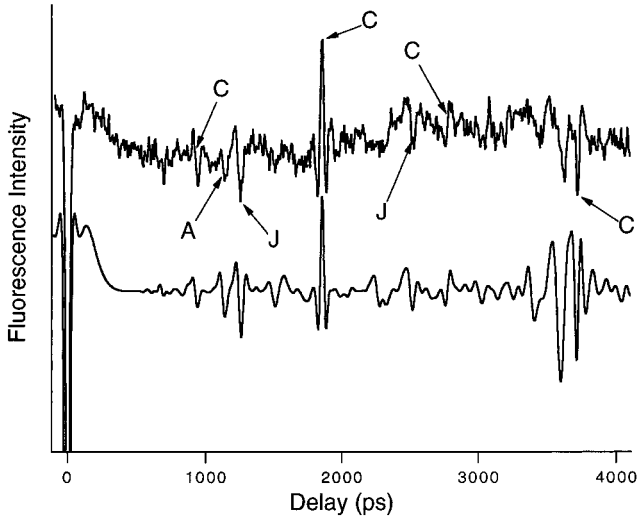

Figure 10. Experimental (top) and calculated (bottom) RCS-TRFD traces for the $h_{10}-h_{12}$ isotopomer of fluorene−cyclohexane. The rotational constants used to calculate the lower trace are given in the second column of Table 7.

we make it based on the fact that the fluorene−benzene binding energy is 275 cm^{-1} larger in the S_1 state than in the S_0 state.[23] The larger binding energy suggests a contraction of the complex and thus an increase in $(A + B)$ upon excitation to S_1. Unambiguous assignment of the vibronic-state-specific rotational constants is not possible due to the degenerate nature of the RCS-TRFD experiment, but such an assignment could easily be obtained from a state-specific RCS experiment.[24]

2. Fluorene−Aliphatic Complexes. RCS results were obtained for four isotopomers of each fluorene−aliphatic complex where the aliphatic molecule was cyclohexane or methylcyclohexane. Figure 10 shows an RCS-TRFD trace for the $h_{10}-h_{12}$ isotopomer of fluorene−cyclohexane, and Figure 11 shows an RCS-TRFD trace for the $h_{10}-h_{14}$ isotopomer of fluorene−methylcyclohexane. The data show two sets of equally spaced transients. The first set of transients is labeled by "J". These

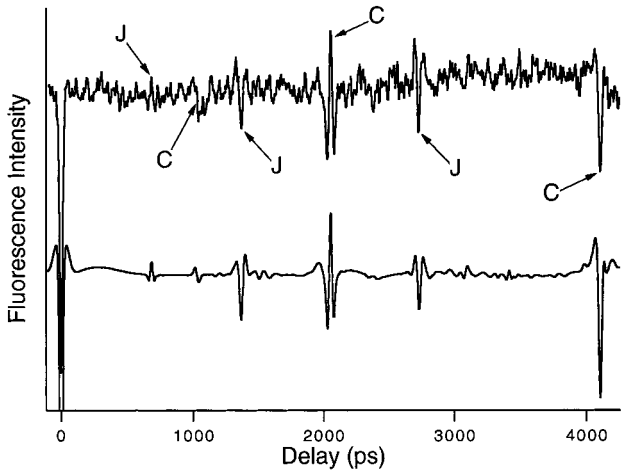

Figure 11. Experimental (top) and calculated (bottom) RCS-TRFD traces for the h_0-h_{14} isotopomer of fluorene−methylcyclohexane. The rotational constants used to calculate the lower trace are given in the third column of Table 8.

have negative polarity. The second set is labeled with "C". These appear with both absorption-like and dispersion-like line shapes. A third reproducible feature, labeled "A", appears for fluorene−cyclohexane at ≃1125 ps. Analogous features were observed for all the isotopomers of the fluorene−aliphatic complexes.

The negative polarity of the "J"-labeled transients suggests that they may be K-type. However, they could also be the second and fourth J-type transients, with the first and third of the series being too small to observe. We favor the latter assignment because one always expects J-type transients to appear in an RCS trace, irrespective of the transition dipole direction or asymmetry of the complex, and there are no other candidates for J-type features in the data. The "C"-labeled transients can be assigned as asymmetry transients based on their line-shape characteristics. They are in fact C-type, as confirmed by the results of simulations (see below). The "A"-labeled feature can also be assigned as an asymmetry transient due to its dispersion-like line shape. Simulations reveal it to be an A-type transient (see below).

To verify the above assignments, RCS simulations were performed by assuming values for the rotational constants and the transition dipole direction for the fluorene−cyclohexane species. A plausible geometry for each complex was obtained by minimizing the interaction energy between monomers using a simple atom−atom pair potential[22] including only repulsive and dispersion interactions. The rotational constants for these geometries were then used to simulate an RCS-TRFD trace. The general features of the experimental results were immediately reproduced by this initial simulation, although the positions of the calculated transients did not agree quantitatively with the observed ones. A series of simulations was then performed in which the rotational constants and transition dipole direction were systematically varied from their initial values. These calculations revealed one set of transients, corresponding to those labeled "J" in Figure 10, whose spacings scale with $(A + B)^{-1}$, showing them to be J-type transients of an oblate-like top. Furthermore, the first and third members (positive polarity) of the J-type sequence appeared with very small magnitudes in the simulations, consistent with the apparent absence of these transients in the experimental data. A set of features similar to the "C"-labeled transients in Figure 10 was also revealed by the simulations. These features were found to be spaced by multiples of $(4C)^{-1}$, behavior showing them to be C-type

TABLE 7: Measured and Calculated Rotational Constants for Fluorene−Cyclohexane. The Estimated Uncertainties in *A, B,* and *C* are ±0.7%, ±0.7%, and ±0.6%. The Geometry Associated with the Calculated Rotational Constants Is Shown in Figure 19

isotopomer	measured (MHz)	calculated (MHz)
$h_{12}-h_{12}$		
A	442	444
B	366	366
C	270	270
$h_{12}-d_{12}$		
A	419	417
B	343	342
C	255	254
$d_{12}-h_{12}$		
A	415	414
B	338	339
C	254	255
$d_{12}-d_{12}$		
A	387	387
B	321	320
C	241	240

transients.[30] Finally, for fluorene−cyclohexane, a feature similar to the "A"-labeled feature in Figure 10 was found to grow in as $(A - B)$ increased (increasing asymmetry), but only for transition dipoles having an appreciable *b*-axis component. It was also found to have a position dependent only on the value of the *A* rotational constant. This behavior confirms the assignment of the feature as an A-type transient[30] in an oblate-like species.

Working with this information, fits to the experimental results were performed to extract the best rotational constants from the data. In the case of fluorene−cyclohexane, all three rotational constants are available from the experimental data. These constants are given in Table 7. For fluorene−methylcyclohexane, due to the absence of an A-type asymmetry transient, values for $(A + B)$ and *C* are available from the experimental data. An upper bound on the value of $(A - B)$ can be obtained by comparing the experimental trace to those simulated at different values of $(A - B)$, with $(A + B)$ and *C* fixed. The rotational constants of fluorene−methylcyclohexane isotopomers so derived are given in Table 8.

IV. Analysis of Geometries

A. Procedures. In this section we present an analysis of the structures of the complexes based on the results obtained from the RCS experiments. To perform this analysis, we make the assumptions that the monomer geometries are unaffected by complexation and that isotopic substitution has no effect on the structures of the complexes. The former allows one to express the moment-of-inertia tensor of a complex in terms of the moments of inertia of its constituent monomers plus six independent coordinates that define the relative position of the monomers in the complex.[20c,29] The six coordinates employed herein are (R, Θ, Φ), the polar coordinates of the center of mass of the "solvent" (benzene, toluene, cyclohexane, or methylcyclohexane) with respect to the "solute"-localized (i.e., perylene or fluorene) coordinate system, and (ϕ, θ, ψ), the Euler angles defining the angular orientation of the solvent-localized coordinate system with respect to that of the solute.[32]

The coordinate systems used for the solutes are depicted in Figure 2. The moments of inertia were taken from ref 28 for perylene and from ref 33 for fluorene. The coordinate systems used for the solvents were all right-handed with the origin at the center of mass of the species. For benzene, the C_6 axis was taken as the *z* axis, and an in-plane C_2 axis bisecting two C-C bonds was taken as the *y* axis. The moments of inertia for benzene were taken from the geometry given by ref 34. For toluene, the direction normal to the phenyl plane was taken as the *z* direction, and the in-plane axis pointing toward the methyl group along the $C-CH_3$ single bond was taken as the *x* axis. The moments of inertia for toluene were taken from ref 35. For cyclohexane, the minimum-energy chair conformation, having C_{3d} symmetry and moments of inertia given by ref 36, was assumed. The *z* axis for the molecule was taken as the C_3 symmetry axis, and the *y* axis was taken to be perpendicular to *z* and to bisect two C−C−C angles. Finally, for methylcyclohexane, the chair conformation with the methyl group in an equatorial position was assumed. The *c* principal axis of the molecule defined the *z* axis, and the normal to the symmetry plane of the molecule was taken as *x* (so that the *x* coordinate of the methyl carbon is zero). The moments of inertia for the species were calculated as per the description in ref 37.

Weighted nonlinear least-squares fits (i.e., minimization of χ^2)[25] to the observed rotational constants of a given complex were performed by using eqs 1 of ref 20c with (R, Θ, Φ) and (ϕ, θ, ψ) as fitting parameters. The rotational constants of all of the isotopomers of a complex were fit simultaneously. The resulting best-fit parameters define the structures that we report below. Several points about the fitting procedure should be noted. First, in each fit nonbonded atom−atom distances were monitored. χ^2 was increased when any such distance was less than the sum of the van der Waals radii of the atoms involved.[38] In this way the procedure was biased against those geometries consistent with the measured rotational constants, yet physically unreasonable on energetic grounds. Second, to sample the six-dimensional χ^2 surface efficiently, diflferent initial values for the six parameters were used in the fits. Third, to assess the uncertainty in a given structural parameter, that parameter was held constant at a series of values while the other parameters were allowed to vary. The values of χ^2 for each fit in such a series were compared to provide an indication of the uncertainty in the fixed parameter. In general, it was found that R, θ, and Φ could be well-determined for each complex. However, the fits were found to be less sensitive to the values for ϕ, θ, and ψ. Thus, the relative angular orientation of the two monomers in a complex is less precisely determined by our experimental results than the relative positions of the monomer centers of mass. These issues will be discussed in more detail below for each specific complex.

We emphasize again that the rotational constants reported in section III refer to averages of the S_1 and S_0 constants of the species, with the one exception of fluorene−benzene. As such, except for fluorene−benzene, the geometries that we report below are intermediate between the ground- and excited-state structures.

B. Perylene Complexes. The geometries consistent with the measured rotational constants for the perylene complexes reveal the following general features. First, all complexes exhibit prolate, near parallel-stacked structures in which the perylene-localized $S_1 \leftrightarrow S_0$ transition moment (the perylene long axis) is parallel to the *a* axis of the complex. Second, the calculated rotational constants for all complexes, recorded in the third column of Tables 1−4, compare well with the measured constants. Third, RCS-TRFD simulations based on the rotational constants and transition dipole direction for the calculated geometry closely match the experimental traces for the complexes, as shown in Figures la, 4, and 6a. The structural

TABLE 8: Measured and Calculated Rotational Constants for Fluorene−Methylcyclohexane. The Estimated Uncertainties in ($A + B$) and C Are Both ±0.5%. The Geometry Associated with the Calculated Rotational Constants Is Shown in Figure 20

isotopomer	measured (MHz)	calculated (MHz)
$h_{12}-h_{14}$		
$(A + B)$	734	733
C	243	243
$(A - B)$	>5, <30	16
$h_{12}-d_{14}$		
$(A + B)$	684	684
C	227	227
$(A - B)$	>5, <30	12
$d_{12}-h_{14}$		
$(A + B)$	681	685
C	231	230
$(A - B)$	>5, <30	27
$d_{12}-d_{l4}$		
$(A + B)$	642	640
C	216	216
$(A - B)$	>5, <30	15

parameters characterizing the perylene complexes are summarized in Table 9.

1. Perylene−Benzene. In our preliminary RCS study of perylene−benzene[12] we reported a geometry for the species close to that predicted by Topp et al.[15] We have performed a new geometry analysis for the complex because RCS results have since become available for the perylene bare molecule.[28a] Figure 12 shows the best-fit geometry whose parameters are given in Table 9. The value of ψ, which has no effect on the rotational constants, was fixed arbitrarily. Values of R between 3.50 and 3.70 Å, of Θ between 6° and 17°, and of $|\theta| < 12°$, together with all possible values of Φ and ϕ, give satisfactory fits to the measured rotational constants. These ranges define the uncertainties in the quoted structural parameters for the complex.

2. Perylene−Toluene. The results of the geometry-fitting procedure for the perylene−toluene complex reveal two structures consistent with the measured rotational constants. These geometries are shown in Figure 13 with structural parameters given in Table 9. For Figure 13a the ranges of possible values for the polar coordinates are 3.50 Å ≤ R ≤ 3.70 Å and −2° ≤ Θ ≤ 12°. The value of Φ does not significantly affect the fits, and its value was fixed at zero. The uncertainties in the Euler angles ϕ, θ, and ψ are ±30°, ±14°, and ±30°, respectively. The second geometry consistent with the measured rotational constants (Figure 13b) is characterized by uncertainties in R, Θ, ϕ, θ, and ψ of ±0.05 Å, ±7°, ±30°, ±16°, and ±30°, respectively. The polar angle Φ was again fixed at zero degrees, as its value did not affect the quality of the fits. The rotational constants for these two geometries are given in the third column of Table 2.

Although the two perylene−toluene geometries of Figure 13 cannot be distinguished on the basis of the RCS results, they do differ in two notable respects: (a) the distance between the perylene and toluene planes is 3.60 Å for the first geometry and 3.70 Å for the second, and (b) the position of the toluene methyl group is above one of perylene's naphthalenic rings in the first geometry and above the "bay" region of the perylene in the second. These differences provide some evidence, albeit nondefinitive, that the first geometry is the actual one. First, the 3.60 Å value for the plane-to-plane distance is closer to the analogous distance in perylene−benzene (3.51 A) than the 3.73 Å value. Second, the methyl group position in the first geometry allows for more atom−atom contacts and, hence, a larger attractive dispersion interaction than arises from the methyl's position in the second geometry. Whichever geometry is the correct one, however, one sees that the near parallel-stacked structural motif characterizes each of them, just as it characterizes the perylene−benzene species.

3. Perylene−Cyclohexane. The geometry found for the perylene−cyclohexane complex is shown in Figure 14; see Table 9 for values of the structural parameters. The ranges of possible values for these parameters are as follows: 4.24 Å ≤ R ≤ 4.49 Å, 5° ≤ Θ ≤ 17°, 30° ≤ Φ ≤ 50°, and $|\theta| < 34°$. Many different values of the Euler angle ϕ were found to be consistent with the data. By symmetry the rotational constants of the complex are independent of ψ. The rotational constants for this geometry are given in Table 3.

4. Perylene−Methylcyclohexane. A geometry consistent with the RCS results on perylene−methylcyclohexane is shown in Figure 15. The estimated uncertainties in R, Φ, and θ are ±0.08 Å, ±15°, and ±8°, respectively. Values of Θ between 7° and 13°, ϕ between −130° and −25°, and ψ between 90° and 140° produce satisfactory fits to the measured rotational constants. The rotational constants corresponding to this geometry are given in the third column of Table 4.

The geometry for perylene−methylcyclohexane in Figure 15 is quite similar to that found for perylene−cyclohexane. The placement of the cyclohexane moiety relative to the perylene center of mass and the tilt of that moiety relative to the perylene ring plane are nearly the same for both complexes. This similarity is not particularly surprising and indicates that the interaction of the cyclohexane moiety with the perylene dominates in determining the structure of the perylene−methylcyclohexane. Unfortunately, as is evident from the uncertainties in ϕ and ψ, the RCS results do not fix the position of the methyl group above the perylene plane very well. Hence, the results are not informative as to the interaction of the methyl moiety with perylene.

C. Fluorene Complexes. The geometries consistent with the measured rotational constants for the fluorene systems reveal the following general features. First, all complexes exhibit oblate structures in which the fluorene-localized $S_0 \rightarrow S_1$ transition moment (the fluorene long axis) is parallel to or has a significant component along the a axis of the complex. Second, the calculated rotational constants for all complexes, recorded in the third column of Tables 5−8, compare well with the measured constants. Third, RCS-TRFD simulations based on the rotational constants and transition dipole direction for the calculated geometry closely match the experimental traces for the complexes, as shown in Figures 9, 10, and 11. The structural parameters characterizing the fluorene complexes are summarized in Table 10.

1. Fluorene−Benzene. Fluorene−benzene is the one complex treated in this paper for which resolvable ground- and excited-state RCS transients have been observed. This situation warrants separate geometry fits for the two vibronic states. In performing these fits we have assumed that the larger of the observed ($A + B$) values corresponds to the S_1 state, as described above. The values of ($A - B$) and ($2C - A - B$) were taken to be the same for the two vibronic states because no transients other than the J-type exhibited resolvable splittings in the RCS data.

Fits to the S_0 constants of fluorene−benzene give the geometry shown in Figure 16. The structural parameters characterizing this geometry, given in Table 10, can take on the following ranges of values and still yield good fits to the

TABLE 9: Structural Parameters for the Perylene Complexes. The Uncertainties Associated with Each Parameter Are Discussed More Fully in the Text. An Asterisk (*) Indicates That the Parameter Was Held Fixed at the Given Value. For These Complexes the Rotational Constants Are Independent of the Value of this Parameter

complex	R (A)	(θ) (deg)	Φ (deg)	ϕ (deg)	θ (deg)	ψ (deg)	figure ref
benzene	3.60	13	35	30	0	90*	12
toluene	3.60	0	0	−49	5	91	13a
toluene	3.74	0	0	−18	10	123	13b
cyclohexane	4.35	14	35	−150	−1	90*	14
methylcyclohexane	4.11	8	14	−73	180	135	15

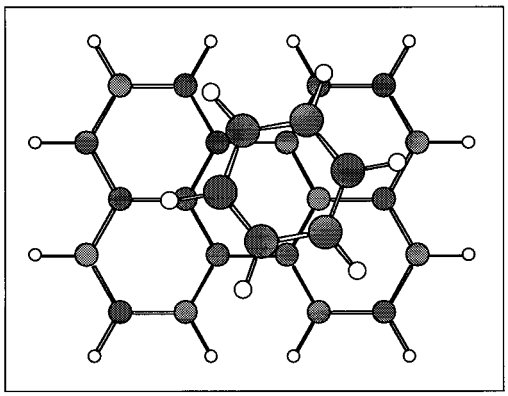

Figure 12. One view of the best-fit calculated geometry for the perylene−benzene complex. Structural parameters for this geometry are given in the text. The rotational constants corresponding to it are given in the third column of Table 1.

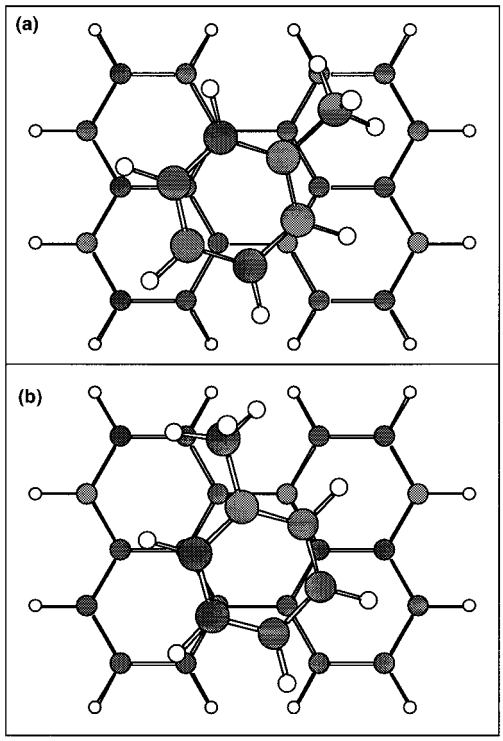

Figure 13. Two geometries for the perylene−toluene complex that are consistent with the RCS results on it. Structural parameters for each are given in the text. Pertinent rotational constants are given in the third and fourth columns of Table 2 for (a) and (b), respectively.

RCS results: 3.98 Å $\leq R \leq$ 4.00 Å, 64° $\leq \Theta \leq$ 72°, −3° $\leq \Phi \leq$ 3°, 160° $\leq \phi \leq$ 200°, and 50° $\leq \theta \leq$ 76°.

Fitting the fluorene−benzene geometry to the S_1 constants measured for the species gives a geometry qualitatively similar to that of Figure 16 with parameters again given in Table 10. The ranges of these parameters consistent with the data are 3.87 Å $\leq R \leq$ 3.89 Å, 64° $\leq \Theta \leq$ 68°, −1° $\leq \Phi \leq$ 1°, 160° $\leq \phi \leq$ 180°, and 60° $\leq \theta \leq$ 74°. Rotational constants for these geometries are compared with the measured values in Table 5.

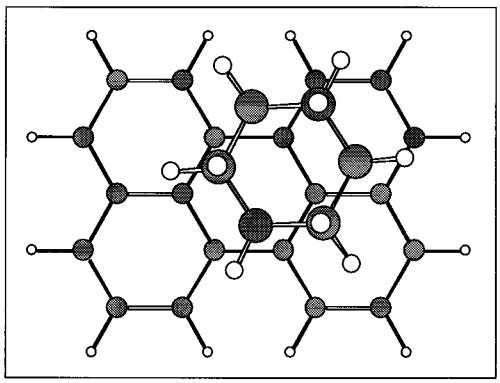

Figure 14. Geometry for the perylene−cyclohexane complex that is consistent with RCS results on it. Structural parameters for the geometry are given in the text. Its rotational constants are given in the third column of Table 3.

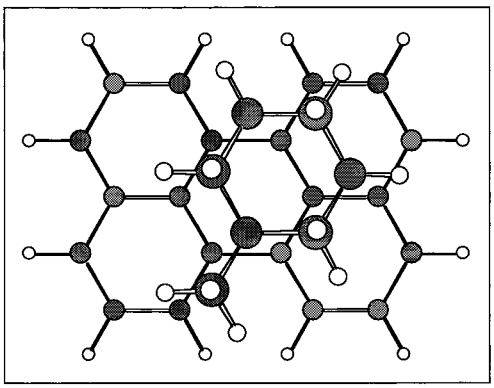

Figure 15. Geometry for perylene−methylcyclohexane that matches the RCS results on the species. Structural parameters for the geometry are given in the text. Its rotational constants are given in the third column of Table 4.

It is important to point out, as described in our previous letter,[11] that, because of the symmetry in fluorene's moment-of-inertia tensor and the near coincidence between the principal axis systems of h_{10}-fluorene and d_{10}-fluorene relative to the fluorene nuclear frame, our RCS results do not permit one to distinguish the geometry of Figure 16 (and the similar S_1 structure) from ones derived from them by rotation of the fluorene moiety by 180° about its *a* principal axis (long axis). This ambiguity characterizes the geometries of all the fluorene-containing species treated herein. Deciding between these two types of structures requires (a) higher-precision measurement of rotational constants than the present ones, (b) rotational results on complexes involving other isotopomers of fluorene, or (c) other kinds of information (e.g., vibrational spectroscopic results). We have chosen to display the particular geometry of Figure 16 because calculations of the minimum-energy structure of the complex by Rosenblum and Speiser[18] indicate that this form is the correct one. Whichever of the two structural forms

TABLE 10: Structural Parameters for the Fluorene Complexes. The Uncertainties Associated with Each Parameter Are Discussed More Fully in the Text. An Asterisk (*) Indicates That the Parameter Was Held Fixed at the Given Value. For These Complexes the Rotational Constants Are Independent of the Value of This Parameter

complex	R (Å)	Θ (deg)	Φ (deg)	ϕ (deg)	θ (deg)	ψ (deg)	figure ref
benzene (S_0)	3.99	67	1	183	65	90*	16
benzene (S_1)	3.88	68	0	173	65	90*	16
toluene	3.87	61	1	181	96	−36	17, 18
cyclohexane	3.98	102	−6	18	103	90*	19
methylcyclohexane	4.02	89	0	6	97	188	20

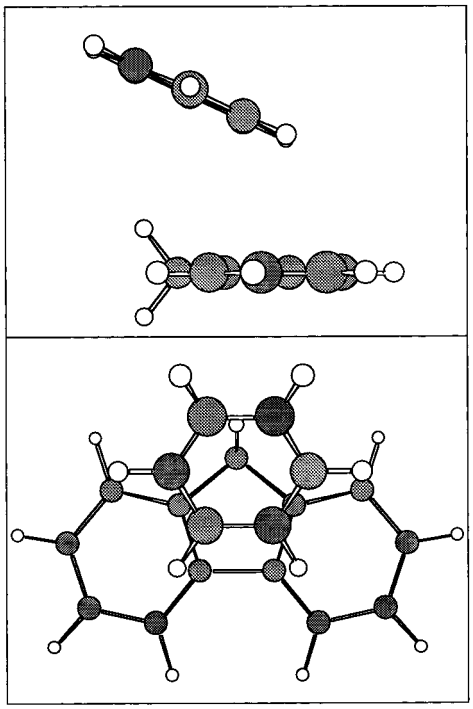

Figure 16. Two views of a geometry for the ground state (S_0) of fluorene−benzene that is consistent with RCS results on the species. Structural parameters corresponding to the geometry are given in the text. Its rotational constants are given in the third column of Table 5.

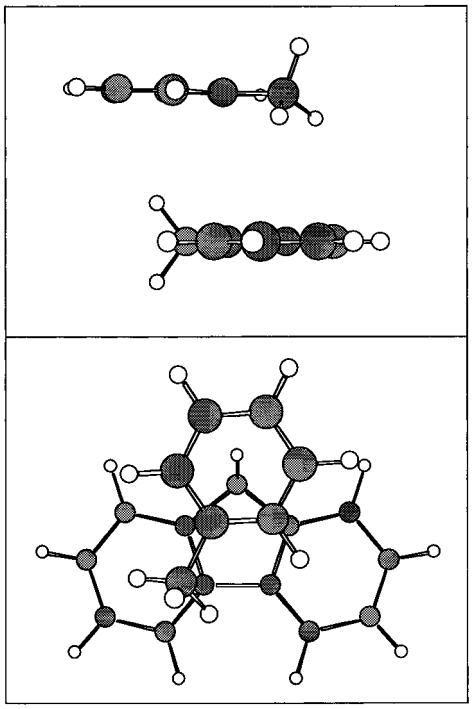

Figure 17. Two views of a geometry of the fluorene−toluene complex that is consistent with RCS results on the species. Structural parameters for the geometry are given in the text. Its rotational constants are given in the third column of Table 6.

is correct, however, one still can make several important points regarding the fluorene−benzene geometries. First, both the S_0 and S_1 structures exhibit a significant tilt (about 25°) of the benzene moiety into the plane of the fluorene molecule. In fact, the uncertainty in θ, the relevant angle, does not allow for geometries having parallel moieties. Second, the benzene center of mass is not directly above the fluorene center of mass. Finally, there is a clear and significant contraction of the complex upon the changing of its electronic state (the value for R changes by 0.11 Å).

2. Fluorene−Toluene. Fits to the rotational constants measured for fluorene−toluene isotopomers yield the geometry shown in Figure 17; see Table 10 for structural paramters. We estimate the uncertainties in the structural parameters as 3.85 Å $\leq R \leq$ 3.89 Å, 60° $\leq \Theta \leq$ 68°, −2° $\leq \Phi \leq$ 4°, 178° $\leq \phi \leq$ 190°, 80° $\leq \theta \leq$ 100°, and −46° $\leq \psi \leq$ −26°. The rotational constants for the geometry of Figure 17 are compared with the measured ones in Table 6.

A second geometry that also gives a good fit to the rotational constants is shown in Figure 18. This one can be derived from that of Figure 18 by rotating the fluorene monomer in that structure 180° about its long axis. As discussed above, the near overlap of the principal axes of perprotonated and perdeuterated fluorene makes it impossible for us to distinguish between the geometries connected by such a transformation based on our RCS results alone. Our best guess for the correct geometry of fluorene−toluene is that represented by Figure 17. We base this conjecture on the minimum-energy structure calculated[18] for fluorene−benzene, together with the expectation that the fluorene−toluene geometry should qualitatively resemble the fluorene−benzene one.

There are three points of note about the fluorene−toluene geometries of Figures 17 and 18. First, the phenyl group in each is in a position close to that of the benzene moiety in one or the other of the two best fit fluorene−benzene geometries (Figure 16 and that derived from Figure 16 by 180° rotation of the fluorene about the long axis). This suggests that the interaction of the phenyl moiety with fluorene is that which dominates in determining the fluorene−toluene geometry. Second, the toluene ring is essentially parallel to the fluorene plane, a point that differs from fluorene−benzene and likely reflects the influence of the methyl moiety. Third, the methyl group is situated above an aromatic ring of the fluorene monomer, indicating an overall attractive interaction between the fluorene and the methyl moiety.

3. Fluorene−Cyclohexane. Fits to the rotational constants measured for the fluorene−cyclohexane complex produce the geometry shown in Figure 19. Estimated uncertainties for the structural parameters given in Table 10 are 3.97 Å $\leq R \leq$ 4.00 Å, 78° $\leq \Theta \leq$ 104°, − 6° $\leq \Phi \leq$ −8°, 0° $\leq \phi \leq$ 26°, and 62° $\leq \theta \leq$ 110°. The rotational constants corresponding to the geometry of Figure 19 are compared with the measured values for fluorene−cyclohexane in Table 7. Notably, the geometry is such that the fluorene-localized transition dipole has com-

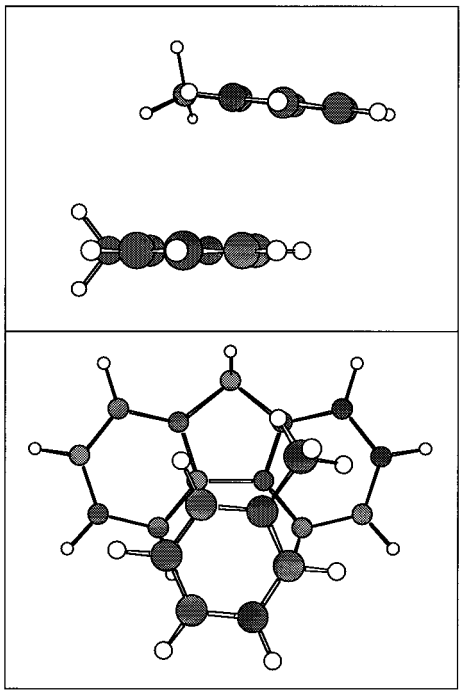

Figure 18. Alternate geometry of the fluorene−toluene complex that is also consistent with RCS results. This geometry can be obtained from that of Figure 17 by rotating the fluorene monomer 180° about its *a* (long) axis.

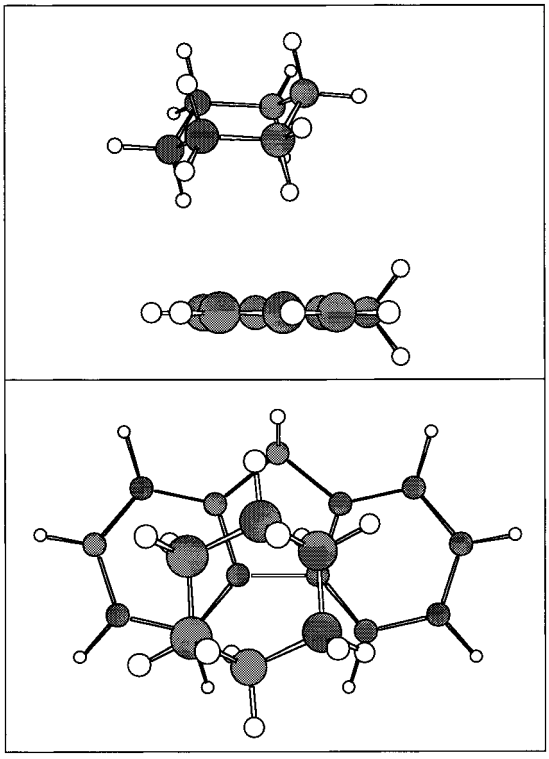

Figure 19. Two views of a geometry of the fluorene−cyclohexane complex that is consistent with RCS results on the species. Structural parameters corresponding to the geometry are given in the text. Its rotational constants are given in the third column of Table 7.

ponents polarized along both the a and b inertial axes of the complex. Such a dipole type is required if both A- and C-type transients are to appear in the RCS results for the complex. Simulations performed by using the rotational constants of the calculated geometry, along with the principal-axis components of the transition dipole associated with that geometry, reproduce

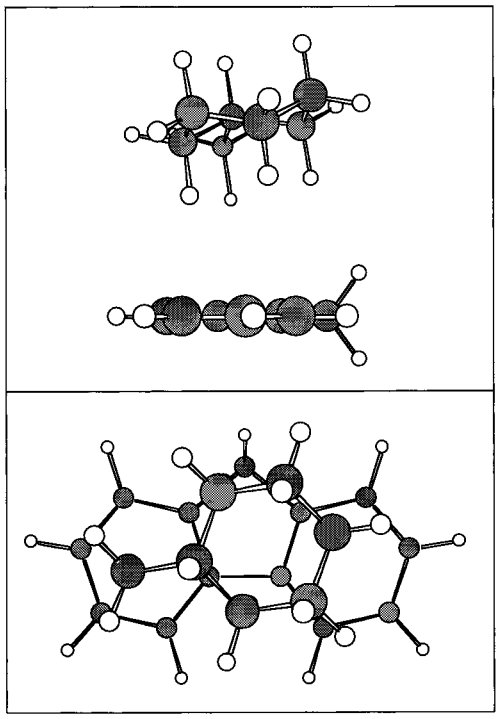

Figure 20. Two views of a geometry of the fluorene−methylcyclohexane complex that is consistent with RCS results on the species. Structural parameters corresponding to the geometry are given in the text. Its rotational constants are given in the third column of Table 8.

the measured RCS traces quite well, as shown in the bottom traces of Figure 10.

Several points should be made about the geometry shown in Figure 19. First, the cyclohexane is close to having its center of mass directly above the fluorene center of mass. This is in contrast to the geometries of both the benzene and toluene complexes of fluorene. Second, within experimental error the C_3 axis of the cyclohexane moiety is perpendicular to the plane of the fluorene moiety. That is, the cyclohexane lies flat, or close to flat, above the fluorene. This contrasts with the geometry of the fluorene−benzene species, in which the tilt of the benzene is real. Finally, as for the benzene and toluene complexes of fluorene, the Figure 19 geometry for fluorene−cyclohexane can be converted into a second distinct one with the same rotational constants by rotating the fluorene moiety by 180° about its *a* axis.

4. Fluorene−Methylcyclohexane. Fitting to the rotational constants measured for the fluorene−methylcyclohexane isotopomers yielded the best-fit structure shown in Figure 20. We estimate the uncertainties in the structural parameters as: 4.01 Å $\leq R \leq$ 4.02 Å, 76° $\leq \Theta \leq$ 102°, − 4° $\leq \Phi \leq$ 4°, −16° $\leq \phi \leq$ 8°, 72° $\leq \theta \leq$ 102°, and 138° $\leq \psi \leq$ 218°. The rotational constants corresponding to this geometry are compared with the measured ones in Table 8.

We note several points concerning the structural results on fluorene−methylcyclohexane. First, as with the fluorene−cyclohexane complex, the cyclohexane moiety is bound close to the center of the fluorene molecule with the "C_3" axis of the cyclohexane moiety perpendicular to the fluorene plane. Second, the RCS results do not fix the position of the methyl group above the fluorene plane very well, as is evident from the range of ψ values consistent with the measured rotational constants. Third, rotation of the fluorene moiety in Figure 20 by 180° leads to a geometry for the complex that also is consistent with the RCS results. The qualitative nature of this new structure is, however, similar to that of Figure 20.

V. Discussion

There are three comparisons between the geometries of the complexes treated herein that are revealing as to the relative contributions of different types of forces in aromatic−aromatic interactions. One such comparison is between the geometries of the perylene−benzene and −toluene species and those of fluorene−benzene and −toluene. The former are essentially parallel-stacked. The latter, however, differ from parallel-stacked in two significant ways: (a) the planes of the aromatics are at appreciable angles with respect to one another and (b) the stacking is significantly off-center. A second comparison is between geometries of the perylene−aromatic and the perylene−aliphatic species. They are qualitatively very similar; both types are centrally bound and have maximal van der Waals contacts between nonbonded atoms. Thus, there is nothing in their geometries to indicate that the aromatic "solvent" species bind any differently to perylene than do the aliphatic ones. This leads into the third comparison, that between the fluorene−aromatic and the fluorene−aliphatic structures. One now notes significant differences when the solvent is aliphatic as opposed to aromatic. The fluorene−aliphatic species are nearly centrally bound with the two monomer moieties lying flat on one another, clearly a different structural form than that of the fluorene−aromatic complexes.

To make sense of these similarities and differences in structure, we consider the three types of intermolecular forces expected to contribute most significantly to the interaction between two aromatic hydrocarbons (see, for example, refs 14−18, 39, 40). These are (a) exchange forces, which are purely repulsive and relatively short-range, (b) dispersion forces, which are purely attractive and fall off as the inverse sixth power of the distance between two nonbonded nuclei, and (c) electrostatic forces between the undistorted charge distributions of the two monomer moieties. The exchange forces serve primarily to limit the distance of closest approach between monomer moieties. They do not favor one particular structural form over others. Dispersion forces favor geometries in which the number of nonbonded atom−atom contacts is maximized. In aromatic−aromatic complexes the dispersion contribution to the binding energy is maximal for parallel-stacked structures. The electrostatic forces in interactions between aromatic hydrocarbons are due primarily to the negative charge clouds corresponding to the π electrons above and below the carbon rings and to the polar nature of the C−H bonds, in which the hydrogen is more positively charged than the carbon. Such charge distributions in two aromatics lead to favorable electrostatic interactions when the edge of one aromatic points into the center of the other.

Unfavorable electrostatic interactions are obtained when the two aromatics are stacked directly above one another with planes parallel. The point is that the minimum-energy structure of a particular complex of two aromatic hydrocarbons is determined by the competition between the dispersion and electrostatic contributions to the interaction energy.

In the light of the above, consider now the qualitative differences in structure between the perylene−aromatic and the fluorene−aromatic species. The parallel-stacked structures of the perylene complexes indicate that dispersion forces dominate over electrostatic ones in the intermolecular interaction. The parallel-displaced tilted structures of the fluorene species are in between the two types of geometries favored by dispersion and electrostatics, respectively. Thus, these structural results suggest a balance between the two forces in the intermolecular interaction.

Further evidence for this interpretation is given by the observed perylene−aliphatic and fluorene−aliphatic structures. The aliphatic species, lacking π electrons, are not subject to $\pi-\pi$ repulsion forces when lying flat on an aromatic solute. They are expected to have, however, dispersion interactions with the solutes that are similar to those characterizing the benzene and toluene complexes with perylene and fluorene. Thus, one can view the gross structures of the aromatic-aliphatic complexes as the kind of geometries that would be obtained in aromatic−aromatic species if $\pi-\pi$ repulsion were not present. The similarity of the perylene−aromatic and perylene−aliphatic structures therefore argues for the relative insignificance of π-cloud repulsion in determining the structures of the former species. Conversely, the significant qualitative differences between the geometries of the fluorene−aromatic and the fluorene−aliphatic species are evidence that such repulsion plays an appreciable role in the fluorene−aromatic interactions.

Final support for the above interpretation derives from calculations of minimum energy geometries of the relevant species. We have performed such calculations by employing a an exp-6 semiempirical atom−atom potential-energy surface,[14] which accounts only for dispersion and exchange repulsion and (b) an exp-6-1 atom−atom potential, which is just the exp-6 surface augmented by Couloumb terms involving atom-centered point charges. The exp-6 parameters were taken from ref 14. The atomic charges were taken from ref 41 for perylene, ref 39 for fluorene, ref 40 for benzene, and ref 42 for toluene. Energy minimization was performed by using the simplex method.[43] For all of the aromatic−aromatic species relevant herein the calculations employing the exp-6 potential predict geometries that are parallel-stacked. When the Coulomb terms are added, however, the predicted fluorene−aromatic geometries are no longer centrally bound and there is a significant angle between the aromatic planes; in short, the calculated structures are qualitatively the same as those observed. In contrast, the perylene−aromatic species have the same gross geometries for both the exp-6 and exp-6-1 potentials. Indeed, both surfaces predict minimum-energy geometries that match the experimental ones qualitatively. The implication is clear: electrostatic interactions are important in determining the geometries of the fluorene-containing species and they are considerably less important in determining those of the perylene-containing ones.

We close by addressing the question of why electrostatic forces (namely, π-cloud repulsion) are more significant relative to dispersion in fluorene−benzene and −toluene than in the corresponding perylene−containing species. The difference can be reasonably attributed to the different number of atoms in perylene and fluorene. The larger number of atoms in the former allows for a greater number of atom−atom interactions in perylene−benzene and −toluene than in the fluorene-containing species. This, in turn, means that the dispersion energy in the former can be greater than in the latter and that, therefore, the relative influence of electrostatic forces will be less for the perylene complexes than for the fluorene ones. Based on this, one predicts that complexes of benzene or toluene with aromatic−hydrocarbon solutes smaller than fluorene will exhibit even more pronounced manifestations of electrostatic forces than are exhibited in fluorene−benzene and −toluene. Indeed, the T-shaped structure of benzene dimer[9,44] bears this prediction out. Conversely, one expects aromatics of the size of perylene or larger to exhibit parallel-stacked structures in interactions with other aromatics.

Acknowledgment. This work was supported by the National Science Foundation (CHE 94-18349), by the Donors of the Petroleum Research Fund administered by the American

Chemical Society (29816-AC6), and by the Department of Energy (DF-FG03-89-ER14066).

References and Notes

(1) Deisenhofer, J.; Epp, O.; Miki, K.; Huber, R.; Michel, H. J. *Mol. Biol.* **1984**, *180*, 385.

(2) Hunter, C. A.; Sanders, J. K. M. *J. Am. Chem. Soc.* **1990**, *112*, 5525.

(3) Rebek, J. *Science* **1987**, *235*, 1478, and references therein.

(4) Wakelin, L. P. *G. Med. Res. Rev.* **1986**, *6*, 275. (b) Neidle, S.; Pearl, L. H.; Skelly, J. V. *J. Biochem.* **1987**, *243*, 1.

(5) Saenger, W. *Principles of Nucleic Acid Structure*; Springer-Verlag: New York, 1984.

(6) For example: Burley, S. K.; Petsko, G. A. *Science* **1985**, *229*, 23.

(7) For example, see: Itoh, M.; Kajimoto, O. In *Dynamics of Excited Molecules*; Kuchitsu, K., Ed.; Elsevier: New York, 1994; p 333.

(8) (a) Levy, D. H.; Haynam, C. A.; Brumbaugh, D. V. *Faraday Discuss. Chem. Soc.* **1982**, *73*, 137. (b) Haynam, C. A.; Brumbaugh, D. V.; Levy, D. H. J. *Chem. Phys.* **1983**, *79*, 1581. (c) Haynam, C. A.; Brumbaugh, D. V.; Levy, D. H. J. *Chem. Phys.* **1984**, *81*, 2282.

(9) Arunan, E.; Gutowsky, H. S. *J. Chem. Phys.* **1993**, *98*, 4294.

(10) For reviews, see: Felker, P. M. *J. Phys. Chem.* **1992**, *96*, 7845. Felker, P. M.; Zewail, A. H. In *Femtosecond Chemistry*, Vol. 1; Manz, J., Wöste, L., Eds.; VCH Verlagsgesellschaft mbH: Weinheim, 1995; p 193.

(11) Joireman, P. W.; Connell, L. L.; Ohline, S. M.; Felker, P. M. *J. Phys. Chem.* **1991**, *95*, 4935.

(12) Joireman, P. W.; Connell, L. L.; Ohline, S. M.; Felker, P. M. *Chem. Phys. Lett.* **1991**, *182*, 385.

(13) (a) Stratton, J. R.; Troxler, T.; Pryor, B. A.; Smith, P. G.; Topp, M. R. J. *Phys. Chem.* **1995**, *99*, 1424. (b) Pryor, B. A.; Andrews, P. M.; Palmer, P. M.; Topp, M. R. *Chem. Phys. Lett.* **1997**, *267*, 531.

(14) Williams, D. E. *Acta Crystallogr. Sect. A* **1980**, *36*, 715.

(15) Doxtader, M. M.; Mangle, E. A.; Bhattacharya, A. K.; Cohen, S. M.; Topp, M. R. *Chem. Phys.* **1986**, *101*, 413.

(16) Price, S. L.; Stone, A. J. *J. Chem. Phys.* **1987**, *86*, 2859.

(17) Jorgensen, W. L.; Severance, D. L. *J. Am. Chem. Soc.* **1990**, *112*, 4768.

(18) Rosenblum, G.; Speiser, S. *J. Chem. Phys.* **1995**, *102*, 9149.

(19) (a) Côté, M. J.; Kauffman, J. F.; Smith, P. G.; McDonald, J. D. *J. Chem. Phys.* **1990**, *90*, 2864. (b) Kauffman, J. F.; Cote, M. J.; Smith, P. G.; McDonald, J. D. *J. Chem. Phys.* **1990**, *90*, 2874.

(20) (a) Connell, L. L.; Corcoran, T. C.; Joireman, P. W.; Felker, P. M. *J. Phys. Chem.* **1990**, *94*, 1229. (b) Connell, L. L.; Ohline, S. M.; Joireman, P. W.; Corcoran, T. C.; Felker, P. M. *J. Chem. Phys.* **1991**, *94*, 4668. (c) Connell, L. L.; Ohline, S. M.; Joireman, P. W.; Corcoran, T. C.; Felker, P. M. *J. Chem. Phys.* **1992**, *96*, 2585.

(21) The elliptical mirror detection system is similar to that described in Spangler, L. H.; Pratt, D. W. *J. Chem. Phys.* **1986**, *84*, 4789.

(22) Amos, A. T.; Cohen, S. M.; Kettley, J. C.; Palmer, T. F.; Simons, J. P. In *Structure and Dynamics of Weakly Bound Complexes*; Weber, A., Ed.; Reidel: Dordrecht, 1987; p 263.

(23) Even, U.; Jortner, J. *J. Chem.* Phys. **1983**, *78*, 3445.

(24) Hartland, G. V.; Connell, L. L.; Felker, P. M. *J. Chem. Phys.* **1991**, *94*, 7649.

(25) Bevington, P. R. *Data Reduction* and *Error Analysis for* the *Physical Sciences*; McGraw-Hill: New York, 1969.

(26) Amirav, A.; Even, U.; Jortner, *J. Chem. Phys.* **1982**, *67*, 1.

(27) Schwartz, S. A.; Topp, M. R. *Chem. Phys.* **1984**, *88*, 5673.

(28) (a) Ohline, S. M.; Joireman, P. W.; Connell, L. L.; Felker, P. M. *Chem. Phys. Lett.* **1992**, *191*, 362. (b) Ohline, S. M.; Joireman, P. W.; Counell, L. L.; Felker, P. M. *Chem. Phys. Lett.* **1992**, *193*, 335.

(29) Joireman, P. W. Ph.D. Dissertation, University of California: Los Angeles, 1993.

(30) Joireman, P. W.; Connell, L. L.; Ohline, S. M.; Felker, P. M. *J. Chem. Phys.* **1992**, *96*, 4118.

(31) Saigusa, H.; Lim, E. C. *J. Phys. Chem.* **1990**, *94*, 2631.

(32) In defining the Euler angles we use the convention of: Zare, R. N. Angular Momentum; Wiley: New York, 1988; pp 77−79. This convention differs from that employed in refs 11 and 12. Hence, the values of ϕ, θ, and ψ, quoted for fluorene−benzene and perylene−benzene in that reference differ from those quoted herein.

(33) Meerts, W. L.; Majewski, W. A.; van Herpen, W. M. *Can. J. Phys.* **1984**, *62*, 1293.

(34) The benzene geometry was consistent with (1) an oblate top having D_{6h} symmetry, (2) C−H bond distances of 1.08 A, and (3) a ground-state rotational *B* constant given by A. Weber in: Weber, A. *Raman Spectroscopy of Gases and Liquids;* Springer-Verlag: Heidelberg, 1979; and references therein.

(35) Rudolph, H. D.; Dreizler, H.; Jaeschke, A.; Wendling, P. Z. *Naturforsch., A* **1967**, *22*, 940.

(36) (a) Ewbank, J. D.; Kirsh, G.; Schäfer, L. *J. Mol. Struct.* **1976**, *31*, 39. (b) Peters, R. A.; Walker, W. J.; Weber, A. *J. Raman Spectrosc.* **1973**, *1*, 159.

(37) The geometry of the cyclohexane ring was taken from ref 36a. Bond lengths and bond angles for the methyl substituent were taken from: Geise, H. J.; Buys, H. R.; Mijlhoff, F. C. *J. Mol. Struct.* **1971**, *9*, 447. The methyl group hydrogens were taken to be eclipsed with respect to the ring C−H bonds.

(38) The van der Waals radii were taken from: Bondi, A. J. *Phys.* Chem. **1964**, *68*, 441.

(39) Im, H. S.; Grassian, V. H.; Bernstein, E. R. *J. Chem. Phys.* **1990**, *94*, 222.

(40) Schauer, M.; Bernstein, E. R. *J. Chem. Phys.* **1985**, *82*, 3722.

(41) Dallinga, G.; Toneman, L. H.; Traetteberg, M. *Rec. Trav. Chim.* **1967**, *86*, 795.

(42) Akiyama, M. *Spectrochim. Acta* **1984**, *40A*, 781.

(43) Press, W. H.; Teukolsky, S. A.; Vetterling, W. T.; Flannery, B. P. *Numerical Recipes*; Cambridge: New York, 1992; Section 10.4.

(44) Henson, B. F.; Hartland, G. V.; Venturo, V. A.; Felker, P. M. *J. Chem. Phys.* **1992**, *97*, 2189.